Mon. Not. R. Astron. Soc. **379,** 647–662 (2007) doi:10.1111/j.1365-2966.2007.11948.x

SuperWASP-North extrasolar planet candidates: candidates from fields 17 h < RA < 18 h

T. A. Lister,[1,2,12★†] R. G. West,[3] D. M. Wilson,[2] A. Collier Cameron,[1] W. I. Clarkson,[4,8] R. A. Street,[5,13] B. Enoch,[4] N. R. Parley,[4] D. J. Christian,[5] S. R. Kane,[1,9] A. Evans,[2] A. Fitzsimmons,[5] C. A. Haswell,[4] C. Hellier,[2] S. T. Hodgkin,[6] Keith Horne,[1] J. Irwin,[6] F. P. Keenan,[5] A. J. Norton,[4] J. Osborne,[3] D. L. Pollacco,[5] R. Ryans,[5] I. Skillen,[7] P. J. Wheatley[10] and J. R. Barnes[1,11]

[1]*SUPA, School of Physics & Astronomy, University of St Andrews, North Haugh, St Andrews, Fife KY16 9SS*
[2]*Astrophysics Group, School of Chemistry & Physics, Keele University, Staffordshire ST5 5BG*
[3]*Department of Physics & Astronomy, University of Leicester, Leicester LE1 7RH*
[4]*Department of Physics & Astronomy, The Open University, Milton Keynes MK7 6AA*
[5]*Astrophysics Research Centre, Main Physics Building, School of Mathematics and Physics, Queen's University Belfast, BT7 1NN*
[6]*Institute of Astronomy, University of Cambridge, Madingley Road, Cambridge CB3 0HA*
[7]*Isaac Newton Group of Telescopes, Apartado de correos 321, E-38700 Santa Cruz de la Palma, Tenerife, Spain*
[8]*Space Telescope Science Institute (STScI), 3700 San Martin Drive, Baltimore, MD 21218, USA*
[9]*University of Florida, PO Box 112005, 211 Bryant Space Science Center, Gainesville, FL, USA*
[10]*Department of Physics, University of Warwick, Coventry CV4 7AL*
[11]*Centre for Astrophysics Research, Science & Technology Research Institute, University of Hertfordshire, Hatfield AL10 9AB*
[12]*Las Cumbres Observatory, 6740B Cortona Drive, CA 93117, USA*
[13]*Department of Physics, Broida Hall, University of California, Santa Barbara, CA 93106-9530, USA*

Accepted 2007 May 2. Received 2007 May 1; in original form 2006 August 25

ABSTRACT

We have performed photometric observations of nearly seven million stars with $8 < V < 15$ with the SuperWASP-North instrument from La Palma between 2004 May to September. Fields in the right ascension range 17–18 h, yielding over 185 000 stars with sufficient quality data, have been searched for transits using a modified box least-squares (BLS) algorithm. We find a total of 58 initial transiting candidates which have high signal-to-noise ratio in the BLS, show multiple transit-like dips and have passed visual inspection. Analysis of the blending and the inferred planetary radii for these candidates leave, a total of seven transiting planet candidates which pass all the tests plus four which pass the majority. We discuss the derived parameters for these candidates and their properties and comment on the implications for future transit searches.

Key words: methods: data analysis – techniques: photometric – surveys – planetary systems.

1 INTRODUCTION

Since the discovery of the first extrasolar planets around pulsars (Wolszczan & Frail 1992) and Sun-like stars (Mayor & Queloz 1995) and the subsequent discovery of over 200 other planets[1] in the following decade, many questions about their formation, evolution and distribution have been raised. In particular, the discovery of the 'hot Jupiters' with orbital periods less than 5 d has produced a large transformation in the theory of planetary formation and migration to explain how objects can be formed far out in the protoplanetary nebula and brought through the disc and stopped at the very small orbital radii observed.

Although a vast majority of extrasolar planets have been discovered using the radial velocity technique, it is the small subset that transit their parent star that have the greatest potential as these are the only ones for which masses and radii can be determined without the $\sin i$ ambiguity. In addition, observations of transits have been used to examine the atmosphere (Charbonneau et al. 2002) and evaporating exosphere (Vidal-Madjar et al. 2003, 2004) of exoplanets, to search for moons and rings (Brown et al. 2001), while long-term observations of transits have the potential to reveal other planets down to Earth masses (Agol et al. 2005).

Since the first discovery of the transiting extrasolar planet (HD 209458b; Charbonneau et al. 2000), many other searches have

★E-mail: tlister@lcogt.net
†Present address-Las Cumbres Observatory.
[1] http://exoplanet.eu/catalog.php.

Table 1. Journal of spectroscopic observations of transit candidates at the CFHT.

Object (1SWASP+)	UT start	Exponent time (s)	Raw S/N	Deconvolved S/N	Comments
		2005 September 23			
J174645.84+333411.9	06:12	600	∼30	∼820	Seeing ∼1.1 arcsec
		2005 September 24			
J174645.84+333411.9	05:45	400	∼30	∼795	Seeing ∼0.8 arcsec
J173403.61+280145.1	06:51	500	∼26	∼720	Seeing ∼0.5 arcsec
J172826.46+471208.4	07:03	300	∼16	∼430	Seeing ∼0.5 arcsec

been instigated with the aim of discovering transiting planets (see Horne 2003 for a review). The low cost of the equipment used to detect HD 209458b and its easily detected, large inflated radius, which still challenges exoplanetary atmospheric theories (e.g. Burrows, Sudarsky & Hubbard 2003; Laughlin et al. 2005), have led to an underestimation of the difficulties of the data reduction needed to reach the required precision over very wide fields (see discussion by Bakos et al. 2004).

The first extrasolar planets to be discovered by the transit method were found by the Optical Gravitational Lensing Experiment (OGLE) project in 2002 (Udalski et al. 2002a,b,c) and five of the systems have been confirmed spectroscopically. However, this task is made more difficult by the faintness ($V \simeq 15$–18) of these stars, necessitating large amounts of time on very large telescopes. Detailed follow-up studies such as atmospheric spectroscopy and *Spitzer* secondary eclipse detections (Charbonneau et al. 2005; Deming et al. 2005, 2006) require brighter targets. The detection of TReS-1 (Alonso et al. 2004) was the first of an extrasolar planet around a bright star from a 'shallow and wide' survey.

The goal of the Wide Angle Search for Planets (WASP) Project and the SuperWASP instruments is to provide a large number of bright ($9 < V < 13$) extrasolar planet candidates to allow meaningful statistical studies to be carried out and allow follow-up to be undertaken with telescopes of moderate aperture. This paper is part of a series (following Christian et al. 2006) describing results of a search for transiting extrasolar planets from the first season of operations in 2004.

Section 2 describes the instrumentation and the observing strategy and the limited spectroscopic follow-up. The data reduction, pipelining and archive extraction stages are described in Section 3. The transit search, candidate filtering and selection procedure are described in Section 4, and the results of the search are discussed in Section 5. Finally, we summarize our findings in Section 6 and give conclusions in Section 7.

2 OBSERVATIONS AND INSTRUMENTATION

2.1 Photometry

The photometric data were obtained with the SuperWASP-North (SW-N) instrument at the Observatorio del Roque de los Muchachos, La Palma, Canary Islands, during 2004 May to September. At this time, the instrument consisted of five cameras is guided by an equatorial fork mount made by Optical Mechanics, Inc. Each camera was made up of a Canon 200 mm, f/1.8 telephoto lens coupled to a Andor Technologies[2] 2048 × 2048 pixel CCD camera which uses a Marconi (now e^{2}v) thinned, back-illuminated CCD with 13.5 μm pixels with Peltier thermoelectric cooling. The resulting plate scale is 13.7 arcsec pixel^{-1}, and each camera has a field of view (FOV) of $7\overset{\circ}{.}8 \times 7\overset{\circ}{.}8$. The equipment is described in greater detail in Pollacco et al. (2006).

The observational strategy was designed to primarily target a band of fields at Dec. $= +28^\circ$ (corresponding approximately to the latitude of La Palma) at 1 h increments in right ascension (RA). The individual cameras were offset from this position by approximately $\pm 3\overset{\circ}{.}5$ in RA and Dec. The fields were chosen to avoid the densest part of the Galactic plane with no fields at RA = 19–20 h. This prevented source confusion and blending with our large pixel scale which has been shown (Brown 2003) to be a significant source of false positives in wide-field transit surveys. Fields within 30° of the Moon were not observed, and eight to 14 fields were observed each night with 30 s exposures at a cadence of ∼8 min.

In all, a total of 165 fields were observed with a variable number of observations per field on 135 nights giving a total of ∼12.9 billion photometric data points being obtained on ∼6.7 million unique objects. This number does not include the 'orphans'; objects detected in the individual CCD frames but which are not present in the photometric catalogue (see Section 3.1) which have been excluded from the analysis.

2.2 Spectroscopy

Follow-up spectroscopic observations of a small number of transit candidates were obtained by one of us (JRB) as part of another observing program using the 3.6-m Canada–France–Hawaii Telescope (CFHT) and ESPaDOnS echelle spectrograph (Donati et al. 1997; Donati 2003) on Mauna Kea, Hawaii, on the nights of 2005 September 23–24. The instrument was configured in spectropolarimetric mode using the 79 gr mm^{-1} grating and the 2 × 4.5 k pixel EEV1 CCD detector, giving $R \sim 63\,000$ and a wavelength coverage over 40 orders of 370–1050 nm. Observations were obtained in Stokes I and exposure time ranged from 300 to 600 s depending on the brightness of the target. A journal of the spectroscopic observations is shown in Table 1.

The data were reduced automatically at the telescope using LIBRE-ESPRIT[3] to perform bias subtraction, flat-fielding, wavelength calibration and order extraction of the polarization information. The reduction process also makes use of the telluric water lines within the echellogram to align the velocity scale to within a few tens of m/s of the heliocentric reference frame.

The extracted spectra were then analysed using the technique of Least Squares Deconvolution (LSD) (Donati & Collier Cameron 1997; Donati et al. 1997; appendix C of Collier Cameron et al.

[2] http://www.andor-tech.com.

[3] http://www.cfht.hawaii.edu/Instruments/Spectroscopy/Espadons/Espadons_esprit.html.

2002) to boost the signal-to-noise ratio (S/N) of the spectra. LSD makes use of the large number of images of photospheric lines recorded in the several hundred nanometres of wavelength range covered by an echelle spectrograph to increase the S/N by a factor of $\sim\sqrt{\text{number of line images}}$. We used a solar G2 line list in the deconvolution process and obtained 4688 images of 3507 lines for the three targets, giving an increase in S/N of ∼27.

3 DATA ANALYSIS

3.1 Data reduction and pipelining

The photometric data were reduced using the WASP0/SuperWASP automated pipeline (Pollacco et al. 2006). Frames are initially classified through a series of statistical tests into bias, dark flat, object and defective frames. Tests specific to each calibration frame type such as the readout noise (for bias frames), dark current (for darks) and the number of saturated pixels and the illumination gradient (for flat fields) are carried out to determine their usability.

Bias and dark frames are then optimally combined using CCDPACK (Draper, Taylor & Allan 2002) into nightly master calibration files. The automated sequences of flat-fields obtained at dusk and dawn, which span a large range of exposure times, are corrected for tilts in the sky illumination (caused by the large FOV), combined with outlier rejection to produce the flat-field and a shutter correction frame. This frame corrects for the uneven illumination pattern caused by the opening and closing of the iris shutter used in the SuperWASP cameras. This is a very small effect ($\lesssim$0.1 per cent) for our 30 s exposures but is included for completeness within the pipeline as it may be used on data where this effect is more pronounced. Master calibration files from previous nights are then combined with weights that decay exponentially over time with a 'half-life' of 14 d.

Science frames have bad pixels masked, are bias- and dark-subtracted, corrected for shutter travel time and flat-fielded using KAPPA (Currie & Berry 1999) and FIGARO (Shortridge et al. 1995) routines. Objects are then detected on the frame using SExtractor (Bertin & Arnouts 1996) as packaged by Starlink. An automated triangle matching algorithm is used to match the catalogue of detected CCD objects with an automatically extracted subset of the Tycho-2 (Høg et al. 2000) catalogue and derive an astrometric solution. The nine coefficient astrometric fit, which allows for fitting of the field centre and barrel distortion, typically has a rms precision of 0.1–0.2 pixels.

The sky level is determined using a quadratic fit with outlier rejection to the sky background with the stellar sources masked out. Aperture photometry is then carried out on all objects that are present in the frame or have an entry in the USNO-B1.0 (Monet et al. 2003) catalogue with a second epoch red magnitude less than 15.0 within the frame. Objects that are detected within the frame by SExtractor but are not present within the catalogue are designated as 'orphans' and are assigned a SuperWASP identifier based on their position and exported into the Flexible Image Transport System (FITS) binary catalogue which is passed to the photometry code. This ensures that detected transient objects are included and measured. Fluxes are then measured in three apertures of radii 2.5, 3.5 and 4.5 pixels and ratios between these fluxes were used to define a 'blending index' to aid in filtering out blended and non-stellar objects.

The frames in each field were then post-processed to correct for primary and secondary extinction with the frame zero-points tied to a set of local secondary calibrators for each field. These local calibrators were produced from stars observed on high-quality, dark moon nights with the magnitudes obtained from the WASP fluxes, transformed through a colour equation relating the instrumental and Tycho-2 magnitudes. Finally, the resulting FITS binary catalogues for each frame are uploaded to the Atlas DataStore operated by Rutherford Appleton Laboratory (RAL) and then ingested by the SuperWASP Data Archive at University of Leicester.

3.2 Field selection and archive extraction

Data for each field were obtained from the SuperWASP Data Archive held at the University of Leicester. The data were extracted for each field and overlapping data from other cameras in adjacent fields were rejected. In addition, we required a star to have at least 500 data points on more than 10 nights and WASP $V \lesssim 13$ in order for it to be included in the transit search. The details of the 13 fields extracted are given in Table 2. The extraction process and the requirements on the minimum number of observations of a star result in a total of ∼186 000 extracted stars from a total of ∼920 000.

Table 2. Coordinates of field centres surveyed in this work.

RA (J2000.0)	Dec. (J2000.0)	Camera (DAS) number	Number of nights	Number of stars	Number of extracted stars	Number of initial candidates	Number of Filtered candidates	Final number of candidates
17 16 00	+31 26 00	3	127	40 438	8656	664	0	0
17 17 00	+23 26 00	4	129	46 860	9516	732	3	1
17 38 00	+55 41 00	5	110	41 081	8201	220	0	0
17 39 00	+47 23 00	2	119	44 388	8791	410	9	2
17 41 00	+40 24 00	1	103	44 175	9851	596	6	2
17 43 00	+31 26 00	2	130	51 411	11 681	619	2	1
17 44 00	+24 27 00	1	113	63 467	13 893	653	6	2
17 44 00	+39 44 00	5	122	48 612	11 033	911	1	1
17 45 00	+10 28 00	1	93	98 296	21 164	1211	8	2
17 45 00	+17 27 00	2	110	84 334	17 818	691	4	1
17 46 00	+25 45 00	5	108	59 452	14 267	656	4	0
18 14 00	+17 27 00	3	110	116 646	24 216	1321	7	1
18 15 00	+09 28 00	4	109	178 561	26 672	1163	8	0
			Totals	917 721	185 759	9847	58[a]	13[a]

[a]Includes three objects detected in more than one field.

4 SELECTION OF CANDIDATES

4.1 Stage 1 – transit searching

The full details of the removal of the systematic errors left in the data after post-processing and the transit search strategy are given in Collier Cameron et al. (2006) but we present a brief summary here.

Although the SuperWASP fluxes are referenced to a set of stable standard stars for each field drawn from Tycho-2 (Høg et al. 2000), there are still small systematic differences in the frame-to-frame zero-point and colour-dependent terms introduced by the broad unfiltered bandpass. We remove these systematics using the SYSREM algorithm (Tamuz, Mazeh & Zucker 2005).

The transit searching code (HUNTSMAN) uses a refined version of the box least-squares (BLS) algorithm (Kovács, Zucker & Mazeh 2002) which has been shown by Tingley (2003) to be the optimal search method. An initial coarse search grid is set up over frequencies (defined in terms of the period, P, with $0.9 \leqslant P \leqslant 5$ d) and transit epochs (T_0) with the transit width (W) calculated at each frequency via Kepler's third law, assuming a stellar mass of 0.9 $M_\odot$. The transit depth (δ) and the goodness of fit statistic, χ^2, are calculated using optimal fitting.

After the coarse grid search, potential transit candidates have to pass a series of tests designed to weed out false positives. The tests that lead to rejection as a potential candidate are as follows:

(i) less than two transits observed;
(ii) reduced χ^2 of the best fit greater than 3.5;
(iii) any phase gaps greater than 2.5× the transit width;
(iv) signal-to-red noise ratio, $S_{\rm red} < 5$;
(v) the ratio of $\Delta\chi^2$ with a transit model to the $\Delta\chi^2$ of an anti-transit model (following Burke et al. 2006) less than 1.5.

The signal-to-red noise ratio ($S_{\rm red}$ – Collier Cameron et al. 2006; Pont 2006) is the ratio of the best-fitting transit depth to the rms scatter when binned on the expected transit duration and gives a measure of the reliability of a transit detection.

Each candidate in the reduced sample that passes the above tests then has the transit parameters of the five most significant peaks in the periodogram refined. In this stage, the pure box function of Kovács et al. (2002) is replaced with a softened version due to Protopapas, Raul & Alcock (2005). This is analytically differentiable with respect to the key transit parameters (P, T_0, W, δ), allowing rapid refinement using the Newton–Raphson method.

If a transit passes all these tests, then it is accepted as an initial transit candidate. The numbers of these for each field are shown in the 'Number of initial candidates' column of Table 2.

One byproduct of the transit searching is an investigation of the transit recovery fraction as a function of period and differing requirements on the number of transits required. The results of this are shown in Fig. 1 for four sample fields with the number of nights observed spanning the range shown in Table 2. The figure gives the probability of at least N transits (for $N = \{3, 4, 6\}$) being present in the data as a function of orbital period. Transits are considered to be present if there are data within the range of phases $\phi < 0.1W/P$ or $\phi > 1 - 0.1W/P$, where W is the expected transit width and P is the orbital period (see section 3.1 of Collier Cameron et al. 2006).

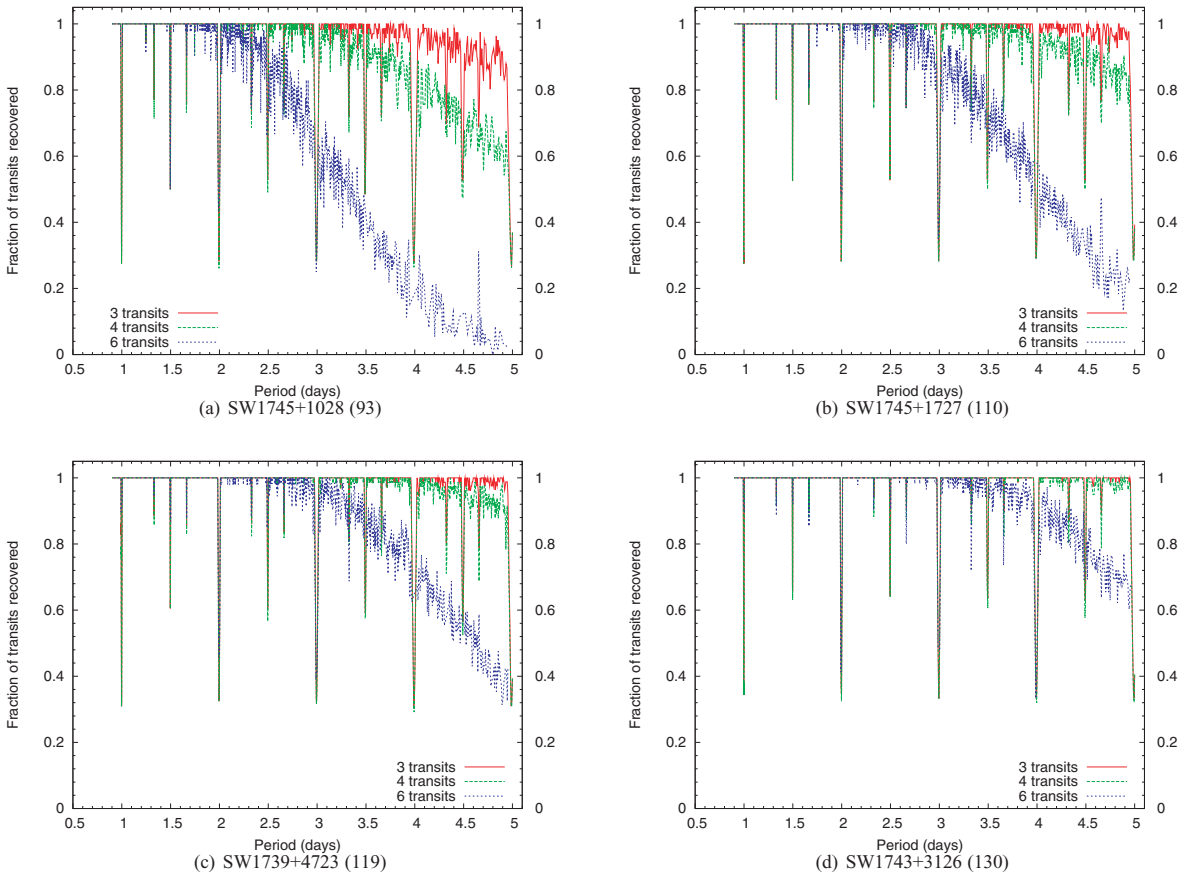

Figure 1. Fraction of transits recovered for four fields with ∼90, 110, 120 and 130 nights observed. Results for three (top curve), four (middle curve) and six (lower curve) detected transits are shown and the number of nights observed is shown in brackets.

4.2 Stage 2 – visual inspection

The transit search described in Section 4.1 produced an initial list of 9847 transit candidates. These were ordered in order of decreasing signal-to-red noise ratio and were all visually inspected. The candidates are identified by their SuperWASP identifiers, which are of the form '1SWASP J*hhmmss.ss*+*ddmmss.s*', with the coordinates based on their position for epoch and equinox J2000.0.

A large fraction (>50 per cent) of the putative transit candidates were caused by defects in the photometry being folded on the 1 d alias and multiples of it. False candidates caused by the 1 d alias were found at periods of ∼2, ∼3, ∼1.5 and ∼1.33 d as well as the normal $P \sim 1$ d. These were rapidly eliminated on casual examination of the light curves and periodograms during the visual inspection process.

During the visual inspection of the transit candidates, any candidates that showed plausible transit shape and depth, remained flat outside of eclipse and were not close to an aliased period, were recorded to be carried through to the next stage. To quantify this somewhat subjective process, we developed the following four-digit coding scheme.

(i) First digit: shape and visibility of the transit.

(a) clear transit-shaped signal of credible width and depth;
(b) shallow/noisy but clearly visible transit signal;
(c) transit barely visible, either very shallow, lost in noise or ill-shaped.
(d) partial transit or gaps around phase 0 but still showing clear transit morphology;
(e) signs of a dip at phase 0 but no clear in/egress.

(ii) Second digit: out-of-transit light curve.

(a) clean and flat, no other variations;
(b) noisy but flat;
(c) signs of ellipsoidal variation or suspected secondary eclipses (includes some candidates which have been folded on twice the period);
(d) shows low-amplitude sinusoidal variation on short timescales, giving a 'knotty' appearance (can indicate that the light curve is folded on the wrong period);
(e) realistic variability of some other form out of transit;
(f) multi-level or 'jumpy' light curves (can indicate the wrong period or photometry artefacts).

(iii) Third digit: distribution of points in the folded light curve.

(a) smoothly sampled with a similar density of points throughout;
(b) some minor regions with slightly lower density of points, retaining a clear signal;
(c) significant clumpiness of data points (can indicate a pathological period).

(iv) Fourth digit: credibility of determined period.

(a) no reason to doubt measured period, clear peak in $\Delta\chi^2$ periodogram;
(b) period gives a secure signal visible in the folded light curve, but peak lies close to a known alias. Sometimes associated with gaps in the folded light curve;
(c) signal visible in folded light curve but period is a known alias or peak lies at a commonly occurring frequency;
(d) light curve suggests that the measured period is wrong.

These codes are shown in the last column of Table 3. We emphasize that these codes are not designed as an 'algorithmic' means of eliminating candidates with a certain code, merely a way to attempt to quantify the subjective visual assessment.

4.3 Stage 3 – filtering

After the candidates for a field have been identified through visual inspection, filtering is performed so that a valid candidate is required to have

(i) signal-to-red noise ratio ($S_{\rm red}$) $\geqslant 8$;
(ii) period greater than 1.05 d;
(iii) more than three transits observed;
(iv) transit to antitransit ratio ($\Delta\chi^2/\Delta\chi^2_- \geqslant 2.0$);
(v) S/N of the ellipsoidal variation ($S/N_{\rm ellip}$) < 8 (based on a cosine fit to the out-of-transit data – see Collier Cameron et al. 2006 for more details).

Following this filtering, the initial candidates were re-sorted into RA order and any groups of objects with very similar transit parameters and SuperWASP identifiers, indicating close proximity on the sky, were investigated using Variable Star Investigator (VSI) (see next section). In all of these cases, the postage stamp images indicated the groups of objects were within the same aperture and therefore almost certainly blended together, and they were removed from the list.

In a few cases, candidates have been carried forward to the next stage of filtering with values of these parameters outside the above ranges. This has generally been in the cases where a value is very close to the cut-off or there has been no evidence for the significant ellipsoidal variation suggested by the $S/N_{\rm ellip}$ value and we have erred on the side of inclusion.

The candidates surviving this filtering are shown in Table 3 along with the other information such as the signal-to-red noise ratio ($S_{\rm red}$) period (P), duration and depth (δ) of the transit, the delta chi-squared of the model ($\Delta\chi^2$), number of transits ($N_{\rm tr}$), the S/N of the ellipsoidal variation ($S/N_{\rm ellip}$) and the transit to antitransit ratio ($\Delta\chi^2/\Delta\chi^2_-$).

The visual inspection process reduced the 9847 initial transit candidates to 199 and the filtering process then further reduced the number of candidates to 58, including three candidates which were detected in more than one field (a total of 55 unique objects). The number of these objects per field is shown in the 'Number of filtered candidates' column of Table 2.

4.4 Stage 4 – additional candidate information

Once filtered transit candidates have been identified from the light curves, we make use of VSI to provide additional information on the transit candidates. VSI was written by one of us (DMW) to query large numbers of astrometric catalogues [USNO-B1.0, Tycho-2, Two Micron All-Sky Survey (2MASS), UCAC-2, PPM], variable object catalogues (*ROSAT*, CCDM, GCVS) and the image servers (DSS, 2MASS; Skrutskie et al. 2006) using the extracted data and atlas images to find blended objects and nearby companions.

VSI also makes use of transit depth, width and period from HUNTSMAN, combined with the colours and radius estimation (Gray 1992; Cox 2000; Ammons et al. 2006) for the extracted stars and the expression from Tingley & Sackett (2005):

$$R_{\rm p} \simeq R_* \sqrt{\frac{\delta}{1.3}},$$

to estimate the planetary radius.

Table 3. Low-amplitude candidate extrasolar planets.

Ident. (1SWASP +)	Period (d)	δ (mag)	Duration (h)	Epoch (2450 000+)	N $_{tr}$	$\Delta\chi^2$	$\Delta\chi^2/\Delta\chi^2_-$	S/N$_{ellip}$	S_{red}	LC code
				Field SW1717+2326						
J165949.13+265346.1	**2.683010**	**0.0209**	**1.824**	**3128.1597**	**13**	**960.5991**	**4.8709**	**9.717**	**12.329**	**1111**
J170319.50+271317.8	1.527922	0.0528	1.656	3128.1069	22	949.4885	4.0610	5.519	12.647	2211
J172515.66+234853.9	1.457706	0.0361	1.440	3128.1826	23	553.5663	4.0588	3.733	10.901	2311
				Field SW1739+4723						
J172117.67+441817.8	1.941607	0.0336	3.912	3137.6143	19	813.7049	3.9546	7.026	12.459	1212
J172302.03+472043.0	4.458795	0.0380	3.264	3136.5464	9	717.0023	2.9865	2.683	12.834	1211
J172336.03+462044.5	1.162678	0.0153	2.232	3138.4099	29	236.8270	3.5019	4.606	9.860	3211
J172549.13+502206.4	**4.542614**	**0.0345**	**1.536**	**3137.4856**	**8**	**569.7906**	**2.8470**	**6.495**	**11.941**	**1211**
(J172826.46+471208.4)[c]	3.405044	0.0217	2.496	3139.1104	7	334.1523	1.1349	1.889	11.967	4121
J173253.52+435009.9	4.557160	0.0287	4.488	3139.5488	8	1263.1642	3.7183	1.259	11.549	2211
J173428.91+471225.3	4.304363	0.0334	2.328	3136.9143	6	139.1181	3.2450	0.773	9.994	2222
J173748.98+471348.7	**3.337786**	**0.0105**	**3.456**	**3139.1697**	**10**	**390.9406**	**4.3549**	**1.028**	**9.895**	**2111**
J174619.33+450103.3	2.403553	0.0295	3.336	3138.1704	15	1442.1517	3.6050	4.681	13.163	1311
J180518.31+460504.9	3.037774	0.0506	2.352	3138.4680	5	1142.2657	14.8579	3.273	10.120	5222
				Field SW1741+4024						
J174116.85+383706.2	4.242378	0.0134	2.832	3138.4702	6	149.0061	3.3432	0.334	11.368	2122
J174118.30+383656.3	**4.245098**	**0.0128**	**3.264**	**3138.4246**	**8**	**137.7380**	**4.8031**	**1.416**	**12.554**	**1211**
J174959.05+370928.8	2.530897	0.0302	5.472	3137.0903	16	729.3705	17.1295	7.504	14.313	1322
J175138.04+381027.5	1.543934	0.0544	2.520	3139.4077	17	6584.2744	14.1000	3.550	14.826	1112
J175207.01+373246.3	1.306420	0.0198	1.032	3138.3350	20	195.1881	1.4261	0.078	11.228	2211
J175856.34+421950.9	**3.256700**	**0.0221**	**2.088**	**3137.7993**	**8**	**430.9857**	**9.0792**	**0.849**	**14.039**	**1211**
				Field SW1743+3126						
J174343.15+340306.5	2.322198	0.0443	4.104	3128.0608	19	2023.3019	5.3088	0.326	10.674	1231
(J174645.84+333411.9)[c]	1.571636	0.0383	1.968	3127.0706	22	10409.9561	52.7193	18.634	24.720	1111
J175401.58+322112.6	**1.949258**	**0.0136**	**1.992**	**3127.8124**	**20**	**225.32**	**3.0137**	**2.911**	**9.440**	**2212**
				Field SW1744+2427						
(J173403.61+280145.1)[c]	4.62676	0.0568	0.192	3126.4275	6	230.8974	4.3579	1.356	15.863	3123
J173508.25+232123.9	2.610171	0.0438	2.088	3126.0015	11	2530.1182	2.3779	0.218	15.612	1111
J174221.53+271435.2	2.104947	0.0253	2.640	3126.7256	14	229.8633	4.5496	1.893	12.803	4212
J175143.72+205953.9	3.069992	0.0145	3.240	3126.0132	10	297.5705	2.1322	2.271	12.900	1211
J175236.10+273225.3	1.905583	0.0298	3.216	3127.1951	21	4562.8867	12.3990	12.173	18.554	1112
J175620.84+253625.7	**4.415010**	**0.0340**	**2.568**	**3124.5637**	**8**	**974.5581**	**15.1208**	**2.012**	**15.219**	**1211**
J180010.55+214510.2	**3.434074**	**0.0557**	**2.184**	**3125.6943**	**8**	**552.4845**	**7.3147**	**0.537**	**16.020**	**1211**
				Field SW1744+3944						
J175856.34+421950.9	**3.258676**	**0.0301**	**2.184**	**3127.9993**	**10**	**431.7925**	**2.4261**	**1.041**	**12.111**	**1212**
				Field SW1745+1028						
J172917.65+065655.0	0.931937	0.0217	1.464	3150.7373	23	445.3489	4.5051	0.581	12.132	2212
J173238.84+104059.9	2.283212	0.0189	2.280	3150.2688	10	191.4931	3.8177	1.191	16.949	4111
J173631.20+133442.9	1.609477	0.0173	1.368	3151.2756	14	225.8527	5.1731	1.606	12.332	2211
J174058.24+062638.1	**4.804517**	**0.0168**	**4.560**	**3146.9646**	**7**	**286.7106**	**2.5973**	**0.845**	**9.583**	**3212**
J174155.92+081459.1	1.228380	0.0363	3.216	3150.6472	22	1211.9445	6.8155	3.168	13.418	2211
J174222.47+101901.5	3.344754	0.0168	3.576	3148.4062	7	173.1803	3.3064	4.469	8.878	2212
J175511.09+134731.5	**2.444503**	**0.0201**	**2.712**	**3149.3391**	**10**	**355.9681**	**7.0766**	**1.328**	**14.494**	**1111**
J175813.15+095151.2	3.746969	0.0488	1.728	3149.6096	6	524.3446	8.5659	1.590	15.826	1221
				Field SW1745+1727						
J174100.71+154714.9	2.147224	0.0551	3.264	3150.0034	14	4797.7295	21.8317	16.977	20.532	1314
J174656.28+143841.2	4.026640	0.0322	2.520	3147.7732	6	271.6478	2.2670	1.491	8.816	2222
J175143.72+205953.9	3.070980	0.0149	3.504	3150.5601	13	366.4742	3.4870	0.186	12.832	1111
J175511.09+134731.5	**2.443916**	**0.0242**	**2.520**	**3149.3479**	**12**	**664.5929**	**4.6498**	**5.335**	**13.218**	**1111**

Table 3 – *continued.*

Ident. (1SWASP +)	Period (d)	δ (mag)	Duration (h)	Epoch (2450 000+)	N $_{tr}$	$\Delta\chi^2$	$\Delta\chi^2/\Delta\chi^2_-$	S/N$_{ellip}$	S_{red}	LC code
				Field SW1746+2545						
J173822.25+290549.2	2.139874	0.0633	3.792	3151.9006	10	918.5665	4.9992	7.531	9.800	1621
J174448.71+273630.5	1.872146	0.0223	2.592	3152.6758	14	1343.4296	5.2142	0.701	13.378	1214
J175236.10+273225.3	1.905144	0.0328	2.928	3151.9788	18	1888.8925	4.1447	21.394	14.569	1112
J180004.71+255947.6	1.238110	0.0212	2.880	3153.4089	24	313.1419	1.5115	2.016	10.483	2211
				Field SW1814+1727						
J175914.99+213803.9	**4.552594**	**0.0302**	**4.224**	**3148.7092**	**4**	**184.8400**	**2.0828**	**0.090**	**8.105**	**2221**
J181022.15+172132.3	1.055949	0.0219	2.424	3150.6555	28	639.9628	7.8049	6.630	15.093	1112
J181113.13+141441.9	3.281877	0.0287	3.360	3148.8628	12	370.3304	7.4041	0.700	12.922	2211
J182330.47+160218.4	1.201000	0.0528	2.232	3151.4124	22	13563.5039	60.1122	8.092	21.624	1111
J182428.52+160346.2	4.258705	0.0476	2.952	3148.2244	6	1289.5090	2.2782	3.331	14.273	1411
J182851.64+200727.2	2.381931	0.0252	2.112	3150.8325	13	351.3000	4.1220	3.022	13.246	2211
J182957.77+174455.2	1.178835	0.0252	2.856	3150.5652	23	965.1992	4.3350	9.531	13.331	2211
				Field SW1815+0928						
J175913.94+132849.4	2.980343	0.0489	3.024	3150.7480	9	4167.3213	18.6379	5.496	12.770	1133
J180202.52+065737.9	1.760327	0.0246	1.968	3150.7300	9	603.1787	7.1428	1.815	12.902	1321
J181222.90+100032.6	1.405853	0.0434	2.232	3151.4324	14	1102.3527	15.8264	1.541	16.583	1111
J181858.42+103550.1	2.464850	0.0124	2.760	3151.1021	10	206.5994	2.7807	0.529	12.086	2122
J182127.51+094038.2	1.832481	0.0145	2.784	3150.8479	11	215.1272	2.1370	1.357	8.855	2111
J182317.92+063936.2	1.854633	0.0300	2.160	3151.1941	13	262.3272	7.5657	1.000	12.530	3212
J182543.36+122925.0	1.390569	0.0539	1.680	3150.7791	15	3254.0181	9.1157	2.034	14.618	1111
J182741.05+082414.0	4.875473	0.0473	4.152	3147.1956	6	441.6472	8.8947	3.500	11.275	2222

($\langle$Id$\rangle$)^c Not selected as a candidate but has spectroscopic data

The factor of 1.3 in the above equation is intended to account for limb-darkening effects. It is derived from Monte Carlo simulations and is strictly only valid for observations in the *I* band but the difference between *I* and our unfiltered wide bandpass is minimal given the errors on the stellar radius when estimated from broad-band colours.

We also use the η_p exoplanet diagnostic from Tingley & Sackett (2005) which is defined as

$$\eta_p \equiv \frac{D_{obs}}{D},$$

where D_{obs} is the observed transit duration and D is the theoretical transit duration. The theoretical duration can be expanded in terms of the period, the planetary radius R_p and the transit depth (see Tingley & Sackett 2005 for further details) enabling η_p to be calculated from the supplied transit parameters and the information extracted from the catalogues. Values close to 1 indicate the observed and theoretical durations agree well and the candidate is more likely to be genuine.

In Table 4, we give the $V_{SW} - K$ colour, the $J - H$ and $H - K$ colours from 2MASS, the inferred stellar radius (R_* in solar radii) and the planetary radius (R_p in Jupiter radii), the exoplanet diagnostic (η_p), the number of brighter (N_{br}) and <5 mag fainter (N_{faint}) objects within the 48 arcsec aperture and a series of letter codes for the plausibility of the planetary radius, exoplanet diagnostic and the degree and the severity of the blending within the 48 arcsec aperture.

The letter codes are as follows:

(i) planetary radius (*R*): values range from A ($R_p < 1.6$), B ($1.6 \geqslant R_p > 1.75$) to C ($R_p \geqslant 1.75$);

(ii) exoplanet diagnostic (Eta): values are encoded as follows A ($0.5 \geqslant \eta_p \geqslant 1.5$), B ($\eta_p < 0.5$), C ($\eta_p > 1.5$);

(iii) blending (B): codes are A (no blends), B (one or two objects less than 5 mag fainter in aperture), C (>2 fainter objects in aperture), D (brighter object in aperture).

It should be noted that candidates having large inferred planetary radii (Codes B and C) could well be interesting in their own right, for example brown dwarf or late M companions.

Those transit candidates that have at least two As and no more than one B or are close to the border between an A and a B with believable transit signals have been designated as 'final transit candidates' and are highlighted in **bold** in Tables 3 and 4. The number of these final transit candidates is also shown in the last column of Table 2.

5 RESULTS

5.1 Candidate light curves

After the blending and the companion radius analysis, we are able to produce a final list of extrasolar planetary candidates for potential follow-up. These are shown in Table 5, where we list the identifier, transit parameters [epoch, period, depth (δ) and duration], stellar parameters [radius (R_*) and spectral type] and derived planet parameters (R_p and η_p), along with a suggested priority for follow-up. This priority is only based on the analysis codes listed above and does not take into account factors such as brightness and visibility of the target. The spectral type has been estimated from the $V_{SW} - K$ colour and the calibration for F, G and K dwarfs by Ammons et al. (2006).

The phase-folded light curves and the periodograms for each transit candidate are shown in Figs 2(a)–(m). In the periodogram plots,

Table 4. Radius and blending results.

Ident. (1SWASP +)	V_{SW} (mag)	$V_{SW} - K$ (mag)	$J - H$ (mag)	$H - K$ (mag)	R_* ($R_\odot$)	R_p (R_{Jup})	η_p	N^a_{br}	N^b_{faint}	Codes[e] R	Eta	Blend
					Field SW1717+2326							
J165949.13+265346.1	**10.951**	**1.50**	**0.22**	**0.08**	**1.08**	**1.33**	**0.61**	**0**	**0**	**A**	**A**	**A**
J170319.50+271317.8	12.944	0.67	0.18	0.06	1.65	3.23	0.49	1	3	C	B	D
J172515.66+234853.9	12.707	0.01	0.32	0.03	2.02	3.27	0.40	1	9	C	B	D
					Field SW1739+4723							
J172117.67+441817.8	12.771	1.50	0.29	0.08	1.08	1.69	1.42	0	0	B	A	A
J172302.03+472043.0	12.575	1.39	0.21	0.06	1.16	1.93	0.86	0	0	C	A	A
J172336.03+462044.5	12.684	2.95	0.64	0.12	0.68	0.72	1.32	0	6	A	A	C
J172549.13+502206.4	**12.033**	**1.70**	**0.30**	**0.09**	**0.97**	**1.54**	**0.45**	**0**	**1**	**A**	**B**	**B/A**
J172824.17+482152.7	10.548	1.09	0.17	0.05	1.37	2.11	0.45	0	0	C	B	A
(J172826.46+471208.4)[c]	11.528	2.05	0.37	0.09	0.82	1.03	0.91	0	0	A	A	A
J173253.52+435009.9	11.345	2.38	0.55	0.11	0.74	1.07	1.55	0	0	A	C	A
J173428.91+471225.3	12.809	N/A	0.32	0.01	1.02[d]	1.59[d]	0.67[d]	4	11	A	A	D
J173748.98+471348.7	**11.442**	**1.62**	**0.33**	**0.06**	**1.01**	**0.88**	**1.16**	**0**	**1**	**A**	**A**	**B**
J174619.33+450103.3	12.087	2.13	0.53	0.10	0.80	1.17	1.36	0	4	A	A	C
J180518.31+460504.9	11.510	2.99	0.62	0.15	0.67	1.29	0.94	0	3	A	A	C
					Field SW1741+4024							
J174116.85+383706.2	11.572	N/A	0.28	0.05	1.10[d]	1.09[d]	0.83[d]	1	7	A	A	D
J174118.30+383656.3	**11.447**	**1.31**	**0.22**	**0.06**	**1.21**	**1.17**	**0.90**	**0**	**1**	**A**	**A**	**B**
J174959.05+370928.8	12.663	2.56	0.55	0.10	0.72	1.07	2.32	0	4	A	C	C
J175138.04+381027.5	11.920	N/A	0.30	-0.00	1.06[d]	2.11[d]	0.96[d]	5	11	C	A	D
J175207.01+373246.3	12.414	1.81	0.36	0.05	0.92	1.10	0.49	0	2	A	B	B
J175856.34+421950.9	**11.619**	**1.54**	**0.28**	**0.06**	**1.06**	**1.34**	**0.66**	**0**	**1**	**A**	**A**	**B**
					Field SW1743+3126							
J174343.15+340306.5	12.587	1.71	0.33	0.09	0.96	1.72	1.48	0	2	B	A	B
(J174645.84+333411.9)[c]	10.904	1.38	0.25	0.04	1.16	1.94	0.73	0	0	C	A	A
J175401.58+322112.6	**12.516**	**1.82**	**0.28**	**0.08**	**0.91**	**0.91**	**0.84**	**0**	**0**	**A**	**A**	**A**
					Field SW1744+2427							
(J173403.61+280145.1)[c]	11.421	1.42	0.23	0.08	1.14	2.32	0.05	0	0	C	B	A
J173508.25+232123.9	11.876	1.57	0.22	0.07	1.04	1.86	0.69	0	0	C	A	A
J174221.53+271435.2	12.985	1.36	0.44	0.01	1.18	1.60	0.90	0	2	B	A	B
J175143.72+205953.9	11.823	2.84	0.51	0.17	0.69	0.71	1.38	0	2	A	A	B
J175236.10+273225.3	11.221	2.35	0.56	0.13	0.75	1.10	1.47	0	9	A	A	C
J175620.84+253625.7	**12.229**	**1.66**	**0.26**	**0.04**	**0.99**	**1.56**	**0.75**	**0**	**2**	**A**	**A**	**B/A**
J180010.55+214510.2	**12.569**	**2.86**	**0.52**	**0.13**	**0.69**	**1.39**	**0.82**	**0**	**4**	**A**	**A**	**C/A**
					Field SW1744+3944							
J175856.34+421950.9	**11.619**	**1.54**	**0.28**	**0.06**	**1.06**	**1.57**	**0.68**	**0**	**1**	**A**	**A**	**B/A**
					Field SW1745+1028							
J172917.65+065655.0	12.288	2.47	0.58	0.15	0.73	0.92	0.88	0	7	A	A	C
J173238.84+104059.9	11.357	1.12	0.25	0.02	1.35	1.58	0.71	0	8	B	A	C
J173631.20+133442.9	12.004	1.61	0.36	0.05	1.02	1.14	0.57	0	4	A	A	C
J174058.24+062638.1	**11.745**	**2.05**	**0.37**	**0.07**	**0.82**	**0.91**	**1.50**	**0**	**2**	**A**	**A**	**B**
J174155.92+081459.1	12.614	2.30	0.62	0.16	0.76	1.24	1.66	0	6	A	C	C
J174222.47+101901.5	12.538	1.38	0.60	0.13	1.16	1.28	1.09	1	12	A	A	D
J175511.09+134731.5	**11.565**	**1.37**	**0.25**	**0.05**	**1.17**	**1.42**	**0.90**	**0**	**0**	**A**	**A**	**A**
J175813.15+095151.2	12.587	1.87	0.29	0.09	0.89	1.68	0.55	0	10	B	A	C

Table 4 – *continued.*

Ident. (1SWASP +)	V_{SW} (mag)	$V_{SW} - K$ (mag)	$J - H$ (mag)	$H - K$ (mag)	R_* ($R_\odot$)	R_p (R_{Jup})	η_p	N^a_{br}	N^b_{faint}	Codes[e] R	Eta	Blend
					Field SW1745+1727							
J174100.71+154714.9	11.653	1.23	0.21	0.05	1.27	2.54	1.01	0	2	C	A	B
J174656.28+143841.2	12.263	0.50	0.36	0.10	1.85	2.83	0.53	3	7	C	A	D
J175143.72+205953.9	11.823	2.84	0.51	0.17	0.69	0.72	1.49	0	2	A	A	B
J175511.09+134731.5	**11.565**	**1.37**	**0.25**	**0.05**	**1.17**	**1.55**	**0.83**	**0**	**0**	**A**	**A**	**A**
					Field SW1746+2545							
J173822.25+290549.2	12.449	0.95	0.30	0.02	1.46	3.13	1.07	1	6	C	A	D
J174448.71+273630.5	10.792	1.19	0.23	0.03	1.30	1.66	0.88	0	1	B	A	B
J175236.10+273225.3	11.221	2.35	0.56	0.13	0.75	1.16	1.33	0	9	A	A	C
J180004.71+255947.6	12.615	N/A	0.07	0.04	1.88[d]	2.34[d]	0.91[d]	1	12	C	A	D
					Field SW1814+1727							
J175914.99+213803.9	12.585	1.86	0.30	0.08	0.89	1.32	1.30	0	4	A	A	C
J181022.15+172132.3	12.661	1.61	0.28	0.12	1.02	1.29	1.15	0	18	A	A	C
J181113.13+141441.9	12.629	1.72	0.27	0.07	0.96	1.39	1.11	0	3	A	A	C
J182330.47+160218.4	11.066	1.17	0.18	0.10	1.31	2.57	0.82	0	2	C	A	B
J182428.52+160346.2	11.788	0.75	0.09	0.08	1.55	2.89	0.65	0	8	C	A	C
J182851.64+200727.2	12.300	1.28	0.23	0.05	1.23	1.67	0.68	0	6	B	A	C
J182957.77+174455.2	12.252	N/A	0.21	0.16	1.25[d]	1.69[d]	1.15[d]	0	25	B	A	C
J183118.99+150600.9	12.472	2.02	0.51	0.10	0.83	1.16	0.91	0	17	A	A	C
					Field SW1815+0928							
J175913.94+132849.4	10.645	1.68	0.18	0.10	0.98	1.85	0.98	0	0	C	A	A
J180202.52+065737.9	10.796	1.76	0.26	0.07	0.94	1.26	0.82	0	5	A	A	C
J181222.90+100032.6	12.196	1.29	0.29	0.06	1.23	2.19	0.82	0	9	C	A	C
J181858.42+103550.1	10.675	1.24	0.17	0.06	1.26	1.20	0.90	0	3	A	A	C
J182127.51+094038.2	11.573	N/A	0.66	0.19	0.63[d]	0.65[d]	1.48[d]	3	29	A	A	D
J182317.92+063936.2	12.289	N/A	0.34	0.09	0.98[d]	1.45[d]	0.85[d]	8	40	A	A	D
J182543.36+122925.0	11.136	1.95	0.30	0.08	0.86	1.70	0.75	0	3	B	A	C
J182741.05+082414.0	12.205	2.72	0.58	0.10	0.70	1.30	1.39	0	4	A	A	C

[a]Number of brighter objects within aperture. [b]Number of objects less than 5 mag fainter within aperture.
(⟨Id⟩)[c]Not selected as a candidate but has spectroscopic data. [d]Based on $J - H$ colour not a $V_{SW} - K$ colour.
[e]Codes: R = planet radius (A = $R_p < 1.6$, B = $1.6 \geqslant R_p > 1.75$, C = $R_p \geqslant 1.75$),
Eta = η_p (A = $0.5 \geqslant \eta_p \geqslant 1.5$, B = $\eta_p < 0.5$, C = $\eta_p > 1.5$),
B = blending (A = OK, B = 1 or 2 fainter objects in aperture, C = >2 fainter objects in aperture, D = brighter objects in aperture).

the dashed vertical lines indicate the main aliased periods of 1 and 2 d. We note the periodograms are not strict Fourier power spectra but rather plots of $\Delta\chi^2$ as a function of trial period and so there is normally little power at the traditional aliased periods of multiples of 1 d.

5.2 Discussion of individual final candidates

5.2.1 1SWASP J165949.13+265346.1

The light curve for this candidate (Fig. 2a) is nicely flat outside of eclipse, despite the supposedly high value of S/N_{ellip} of 9.717, with a well-defined transit. There is a strong signal in the periodogram at the period and a large number (13) of transits were detected. The measured transit duration (1.824 h) is a little small for the size of the planet, leading to a somewhat small value of η_p of 0.61. The only objects within the 48 arcsec aperture are six magnitudes or more fainter and make it unlikely that blending is the cause of the low η_p value. The candidate merits further follow-up.

5.2.2 1SWASP J172549.13+502206.4

The light curve for this object (Fig. 2b) has some scatter and the transit shape is quite narrow and *V* shaped. The inferred stellar radius and moderately large transit depth lead to a quite large planetary radius of $1.54\,R_{Jup}$ with a correspondingly small value of η_p. This combined with the relatively high value of $S/N_{ellip} = 6.495$ could make the companion a low-mass star. There is a 4.5 mag fainter object on the edge of the aperture 46 arcsec away.

5.2.3 1SWASP J173748.98+471348.7

This candidate has a flat light curve although the transit is quite shallow. The estimated planetary radius is quite small at $0.88R_{Jup}$ but is close to what is expected from the duration ($\eta_p = 1.16$) and probably within the errors propagated from the colour indices. There is a 4.3 mag fainter object towards the edge of the aperture 43 arcsec away. The transit appears to be flat bottomed in the folded light curve

Table 5. Final list of candidate planets. Note two objects appear twice in different fields.

Ident. (1SWASP+)	Field	Epoch (2450 000+)	Period (d)	δ (mag)	Duration (h)	N $_{tr}$	R_* ($R_\odot$)	R_p (R_{Jup})	η_p type	Sp.	Priority
J165949.13+265346.1	SW1717+2326	3128.1597	2.683010	0.0209	1.824	13	1.08	1.33	0.61	G1	1
J172549.13+502206.4	SW1739+4723	3137.4856	4.542614	0.0345	1.536	8	0.97	1.54	0.45	G5	2
J173748.98+471348.7	SW1739+4723	3139.1697	3.337786	0.0105	3.456	10	1.01	0.88	1.16	G3	1
J174058.24+062638.1	SW1745+1028	3146.9646	4.804517	0.0168	4.560	7	0.82	0.91	1.50	K0	2
J174118.30+383656.3	SW1741+4024	3138.4246	4.245098	0.0128	3.264	8	1.21	1.17	0.90	F8	1
J175401.58+322112.6	SW1743+3126	3127.8124	1.949258	0.0136	1.992	20	0.91	0.91	0.84	G8	1
J175511.09+134731.5	SW1745+1028	3149.3391	2.444503	0.0201	2.712	10	1.17	1.42	0.90	F9	1
J175511.09+134731.5	SW1745+1727	3149.3479	2.443916	0.0242	2.520	12	1.17	1.55	0.83	F9	1
J175620.84+253625.7	SW1744+2427	3124.5637	4.415010	0.0340	2.568	8	0.99	1.56	0.75	G4	1
J175856.34+421950.9	SW1741+4024	3137.7993	3.256700	0.0221	2.088	8	1.06	1.34	0.66	G1	1
J175856.34+421950.9	SW1744+3944	3127.9993	3.258676	0.0301	2.184	10	1.06	1.57	0.68	G1	1
J175914.99+213803.9	SW1814+1727	3148.7092	4.552594	0.0302	4.224	4	0.89	1.32	1.30	G8	2
J180010.55+214510.2	SW1744+2427	3125.6943	3.434074	0.0557	2.184	8	0.69	1.39	0.82	K5	2

and this candidate deserves spectroscopic follow-up to determine the true nature of the object.

5.2.4 1SWASP J174058.24+062638.1

There is some scatter in the light curve (Fig. 2d) and the transit is somewhat shallow, but there is a quite strong peak in the periodogram. The observed duration of the transit is long for an estimated planet radius $\lesssim R_{Jup}$, leading to a high value of η_p (1.50) indicating this may be a grazing incidence stellar binary. There are two objects 4.3 and 4.9 mag fainter at a distance of 34 and 47 arcsec from the candidate, respectively. The combination of these factors makes this object a lower priority target.

5.2.5 1SWASP J174118.30+383656.3

The transit in this object is quite obvious and there is quite a strong signal in the periodogram from the eight detected transits. The derived spectral type of F8 leads to a quite large stellar radius but the measured transit duration is close to what is expected ($\eta_p = 0.90$) and the planetary radius is reasonable at $1.17R_{Jup}$. There is a very small degree of blending with a 3.5 mag fainter object 19 arcsec away and this could be a grazing incidence stellar binary with similar components on twice the period. Overall, this candidate would merit further follow-up.

5.2.6 1SWASP J175401.58+322112.6

The light curve (Fig. 2f) shows a fair amount of scatter due to the relative faintness of the object ($V_{SW} \sim 12.5$), but the transit is readily visible. The period is somewhat close to the $P = 2$ d alias and it is possible the object may be a false positive, despite the large number of detected transits. The derived planetary radius ($0.91R_{Jup}$) and η_p (0.84) are both reasonable and there is no evidence of any blends. The object is worthy follow-up with the above caveats.

5.2.7 1SWASP J175511.09+134731.5

This candidate is detected in two different fields from different cameras which overlap slightly: SW1745+1028 (DAS 1) and SW1745+1727 (DAS 2). The light curves (Figs 2g and h) look very similar with a clear transit signature and the derived parameters also agree quite well. The determined periods are very similar with small differences in the fitted transit depth leading to small differences in the derived planetary radius ($1.42R_{Jup}$ versus $1.55R_{Jup}$). The derived radii are on the large side for a planet but the calculated transit duration is close to the measured one ($\eta_p \sim 1$). This candidate could be planet or possibly a brown dwarf and warrants further follow-up.

5.2.8 1SWASP J175620.84+253625.7

The transit is clearly visible in the light curve (Fig. 2i) although it has something of a '*V* shape'. The large amplitude ($\delta - 0.0340$) leads to a fairly large planet radius of $1.56R_{Jup}$. This may indicate that the companion is actually stellar although the S/N_{ellip} value is low at 2.012 and the light curve is very flat outside of transit. Additional observations would help to secure the exoplanetary nature of the companion.

5.2.9 1SWASP J175856.34+421950.9

This candidate is detected in two different fields from different cameras which overlap slightly: SW1741+4024 (DAS 1) and SW1744+3944 (DAS 5). The light curves (Figs 2j and k) look very similar and the derived transit parameters also agree quite well with only slight differences in the derived transit depth (0.0221 in field SW1741+4024 compared to 0.0301 in SW1744+3944) leading to small differences in the derived planetary radius ($1.34R_{Jup}$ versus $1.57R_{Jup}$). The transit egress for the light curve from the SW1744+3944 field is somewhat clearer and more pronounced which probably accounts for the somewhat deeper transit amplitude fitted to these data. The only object within the aperture is ~4.8 mag fainter and 26 arcsec away and this candidate would warrant spectroscopic follow-up.

5.2.10 1SWASP J175914.99+213803.9

There is a fair amount of scatter in this faint candidate and only four transits were detected, although there is a clear peak in the periodogram. The derived R_p and η_p are quite large for the size of the star ($1.32R_{Jup}$ and 1.30, respectively) and there is a 3.1 mag fainter object ~19 arcsec away and several other faint sources with the SuperWASP aperture so blending cannot be totally ruled as a cause of the variations.

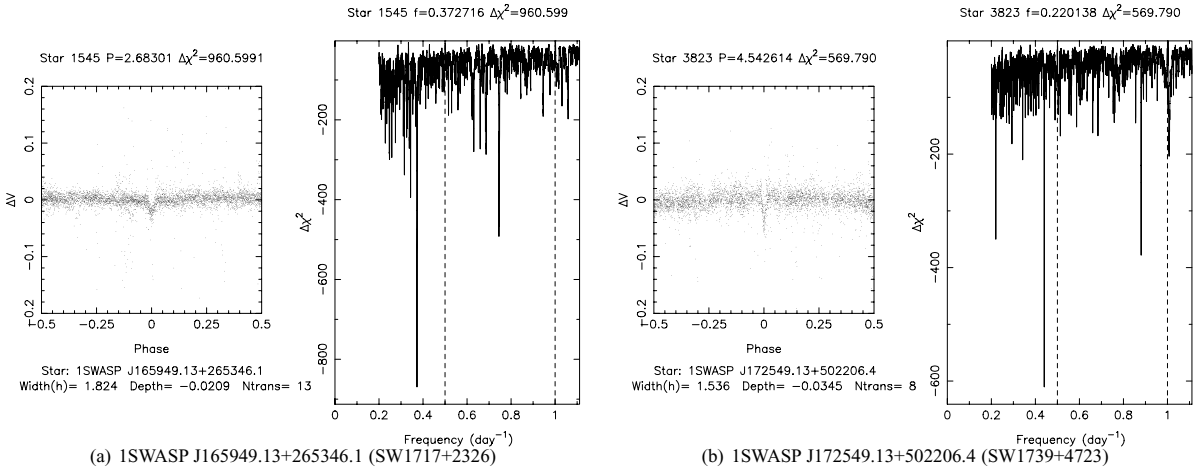

(a) 1SWASP J165949.13+265346.1 (SW1717+2326)

(b) 1SWASP J172549.13+502206.4 (SW1739+4723)

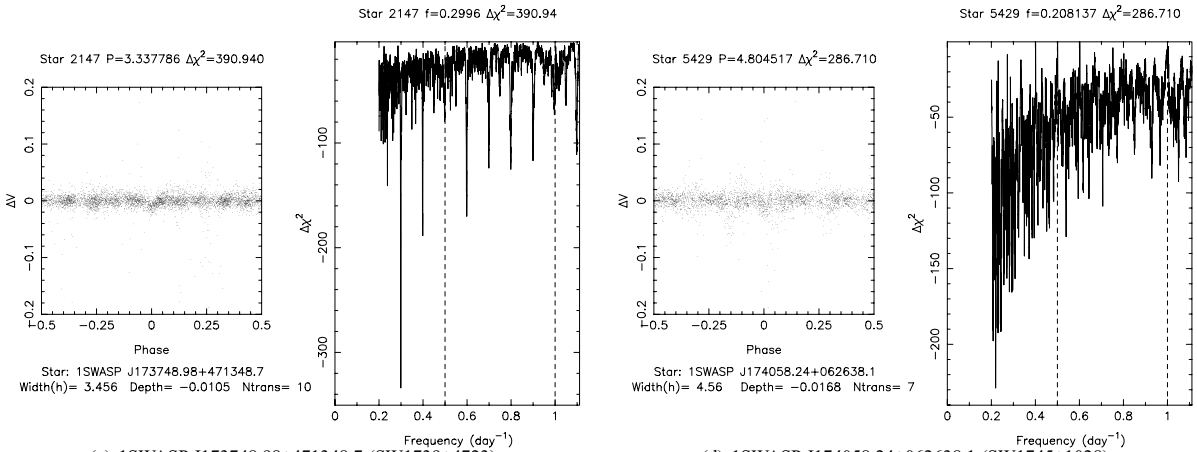

(c) 1SWASP J173748.98+471348.7 (SW1739+4723)

(d) 1SWASP J174058.24+062638.1 (SW1745+1028)

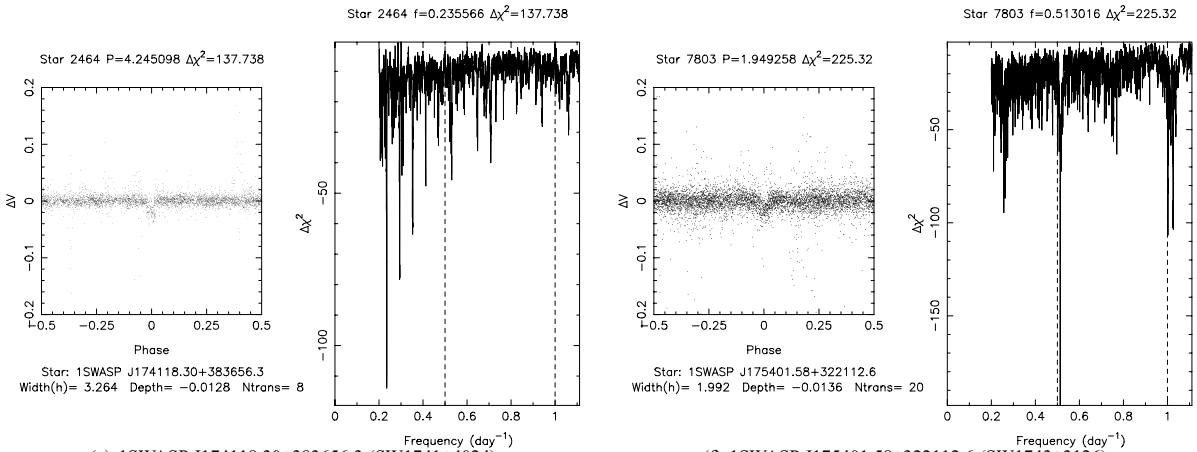

(e) 1SWASP J174118.30+383656.3 (SW1741+4024)

(f) 1SWASP J175401.58+322112.6 (SW1743+3126)

Figure 2. Light curves and periodograms for filtered transit candidates.

5.2.11 1SWASP J180010.55+214510.2

This candidate has the largest depth (0.0557 mag) of any of the candidates although this is partly due to the late spectral type of K5 and small stellar radius, which lead to a planetary radius of $1.39R_{\rm Jup}$. The transit is somewhat undersampled and duration is quite short but the host star has a small stellar radius ($0.69\,{\rm R}_{\odot}$). There are a few objects within the aperture although all are at least 3.25 mag fainter. Although faint and somewhat noisy (see Fig. 2m), this candidate orbits an interestingly late spectral type parent star and would warrant further investigation.

5.3 Discussion of other candidates

5.3.1 1SWASP J175143.72+205953.9

This object is the third that has been detected in two different overlapping fields: SW1744+2427 (DAS1) and SW1745+1727

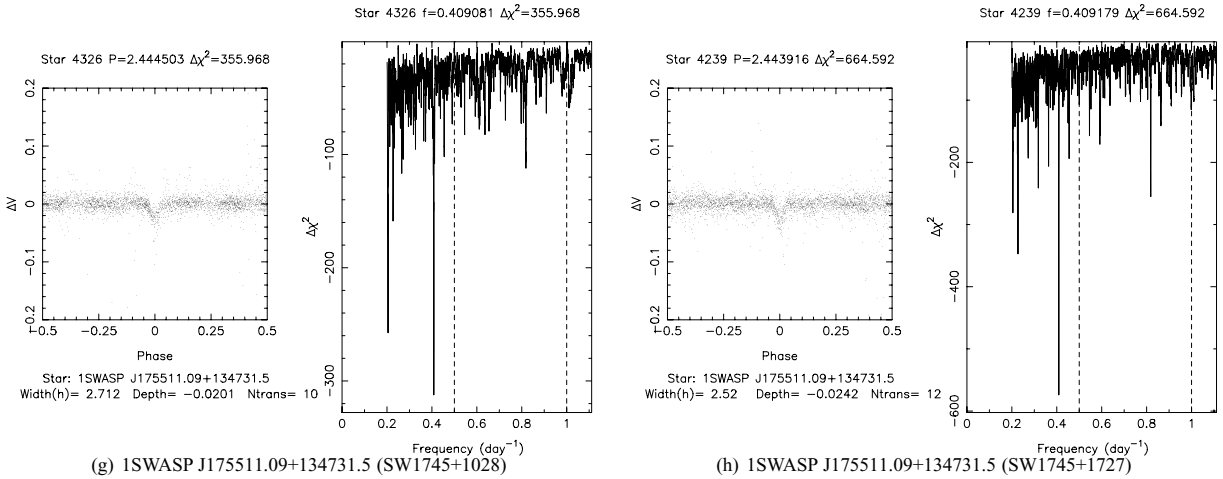

(g) 1SWASP J175511.09+134731.5 (SW1745+1028) (h) 1SWASP J175511.09+134731.5 (SW1745+1727)

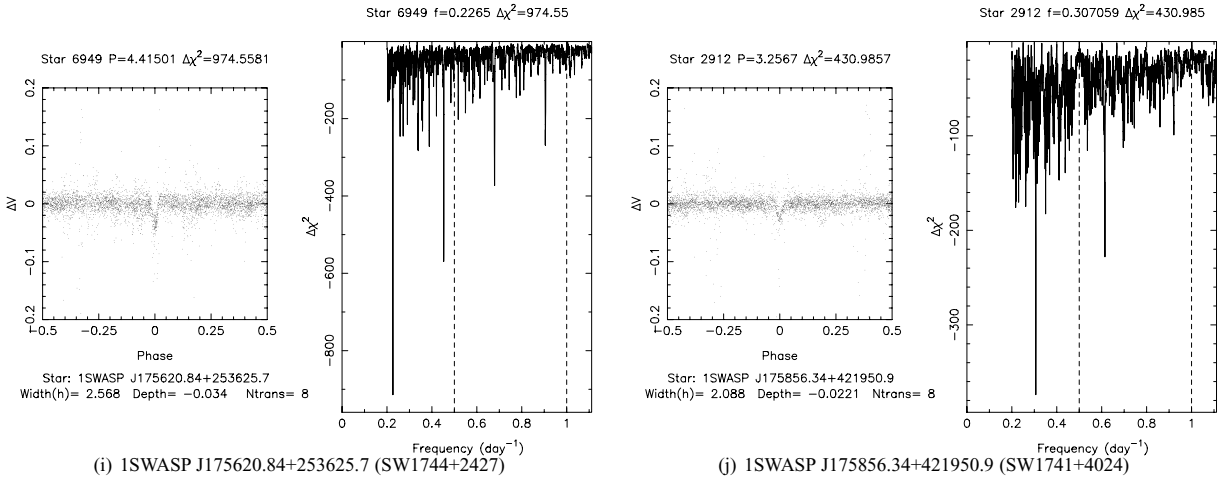

(i) 1SWASP J175620.84+253625.7 (SW1744+2427) (j) 1SWASP J175856.34+421950.9 (SW1741+4024)

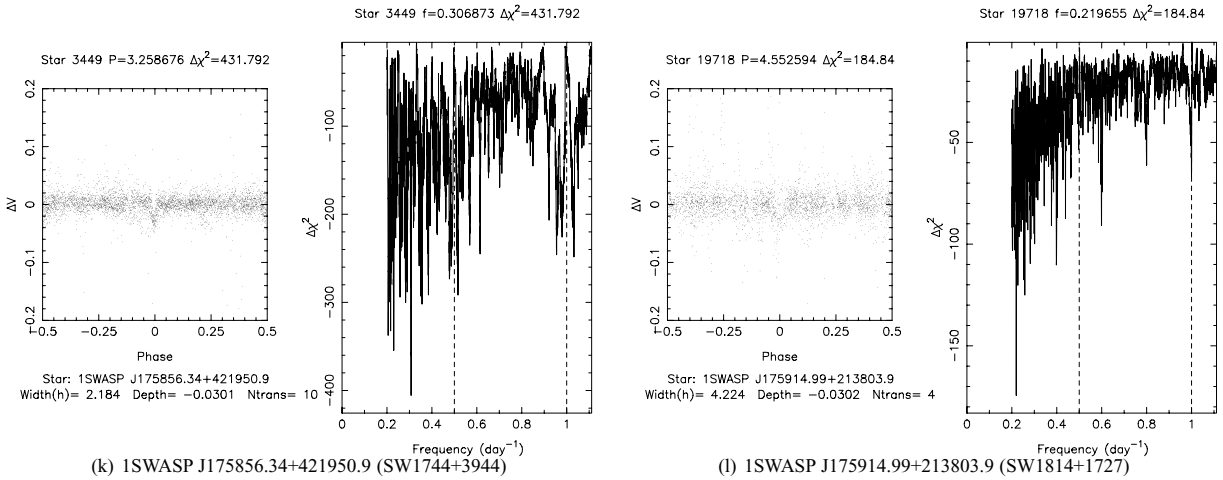

(k) 1SWASP J175856.34+421950.9 (SW1744+3944) (l) 1SWASP J175914.99+213803.9 (SW1814+1727)

Figure 2 – *continued.*

(DAS2). The transit is readily visible in both light curves although the data are somewhat noisy. The derived transit parameters are very similar with depths of 0.0145 and 0.0149 mag leading to a rather small predicted planetary radius of 0.71 and 0.72$R_{\rm Jup}$ when combined with the 0.69 $R_{\odot}$ host star radius.

Although the candidate has only two objects less than 5 mag fainter within the 48 arcsec aperture, one of these objects is ∼3 mag fainter and only 6.5 arcsec away. Examining the DSS image shows an elongation of the candidate and the 2MASS J, H and $K_{\rm s}$ atlas images show the close companion as an additional source touching the candidate. With these caveats, we cannot recommend this target for follow-up although it otherwise passes all the tests. We include the light curve from the SW1744+2427 in Fig. 2(n) for reference.

5.4 Discussion of spectroscopically observed candidates

In this section, we discuss the three objects that have been observed spectroscopically. These objects were observed based on the

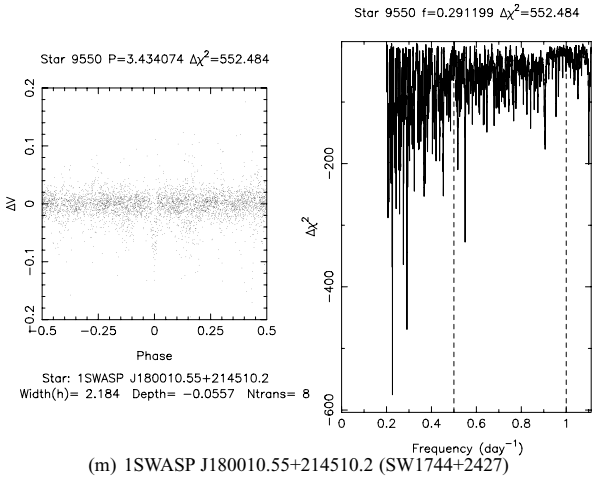

(m) 1SWASP J180010.55+214510.2 (SW1744+2427)

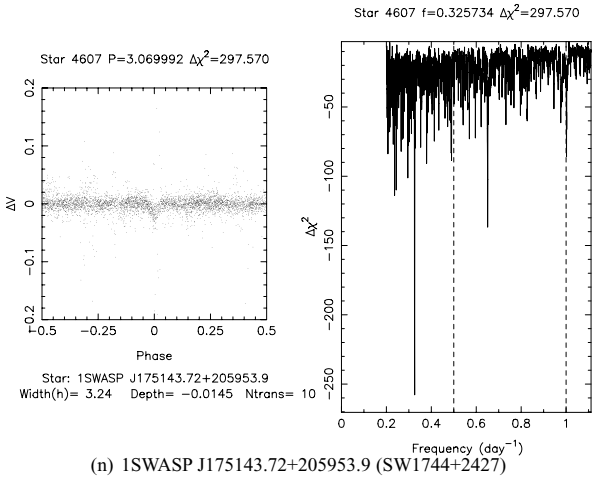

(n) 1SWASP J175143.72+205953.9 (SW1744+2427)

Figure 2 – *continued.*

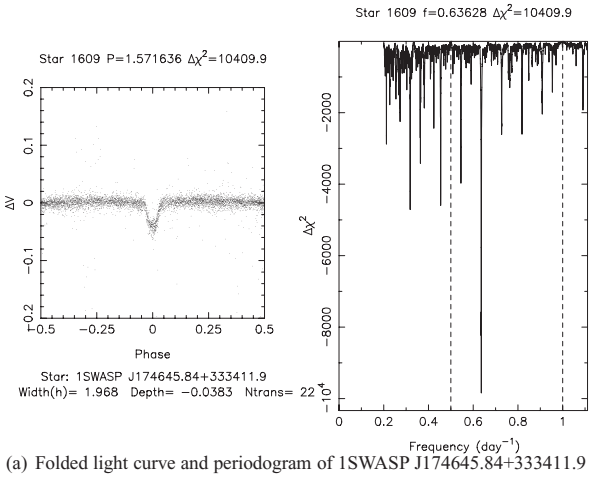

(a) Folded light curve and periodogram of 1SWASP J174645.84+333411.9

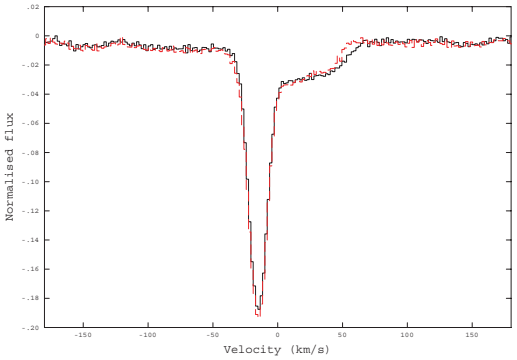

(b) Deconvolved spectrum of 1SWASP J174645.84+333411.9 obtained at the CFHT showing blending with a rapidly-rotating component. The black solid line denotes the spectrum obtained on 23 Sep and the red dashed line is the spectrum obtained on 24 Sep.

Figure 3. Light curve, periodogram and deconvolved spectrum of 1SWASP J174645.84+333411.9.

identification in an earlier transit search carried our on a smaller subset of the data but were not selected in the more rigorous selection and filtering process presented here. The details of the stars are included in parentheses in Tables 3 and 4 but they are not included in the count of filtered candidates in Table 2.

5.4.1 1SWASP J174645.84+333411.9

This object, which has one of the highest $\Delta\chi^2$ found in the transit search, was discovered in preliminary transit searches on a small subset of the data and was included in the list of stars observed with the CFHT and ESPaDOnS. It was also clearly identified in this search of the full data set, although the high S/N_{ellip} value of 18.634 means it fails the filter procedure described in Section 4.4.

The light curve and periodogram are shown in Fig. 3(a) illustrating the clear transit signature and strong periodogram peak which lead to the initial selection. The deconvolved profile is shown in Fig. 4(b) and clearly shows blending with a rapidly rotating component. The derived colour and radius of the primary star and the inferred companion radius from Table 4 of $1.94\,R_{\rm Jup}(\simeq 0.2\,{\rm R}_{\odot})$ indicate that this object is likely to be a short period late F+M stellar binary.

This object (as BD+33° 2954) was also detected by the Hungarian-made Automatic Telescope (HAT) project (Bakos et al. 2004) which also ruled it out as a transit due to the depth of the transits and low-amplitude sinusoidal variation. They also concluded the companion was likely to be a M dwarf.

5.4.2 1SWASP J172826.46+471208.4

This object was identified as a possible candidate during visual inspection in the full data set, but failed the selection cuts described in Section 4.4 due to only having $\Delta\chi^2/\Delta\chi^2_- = 1.13$, less than the 2.0 required. The deconvolved profile is shown in Fig. 4(b) and clearly shows a double-lined signature indicating that it is a stellar binary.

The derived stellar and the planetary parameters are shown in Table 4 for comparison purposes and indicate the value of the high-resolution spectrum. The planetary radius ($1.03R_{\rm Jup}$) and $\eta_{\rm p}$ value of 0.91, combined with the absence of any brighter or fainter companions, would otherwise lead to it having been considered a good candidate.

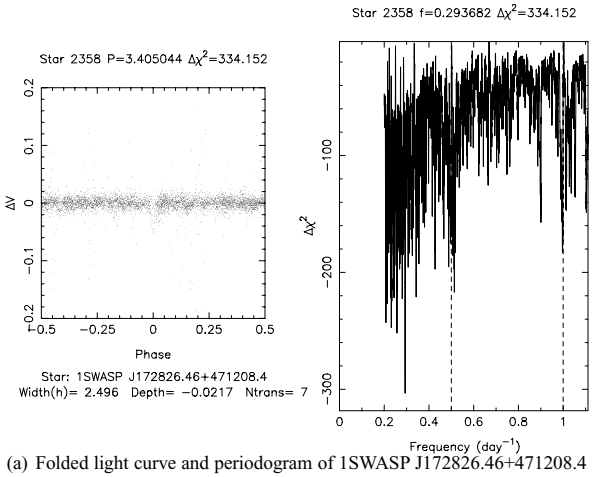

(a) Folded light curve and periodogram of 1SWASP J172826.46+471208.4

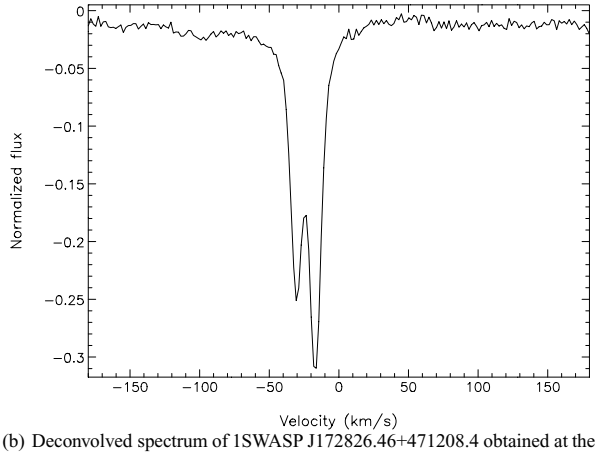

(b) Deconvolved spectrum of 1SWASP J172826.46+471208.4 obtained at the CFHT clearly showing a double-lined spectrum.

Figure 4. Light curve, periodogram and deconvolved spectrum of 1SWASP J172826.46+471208.4.

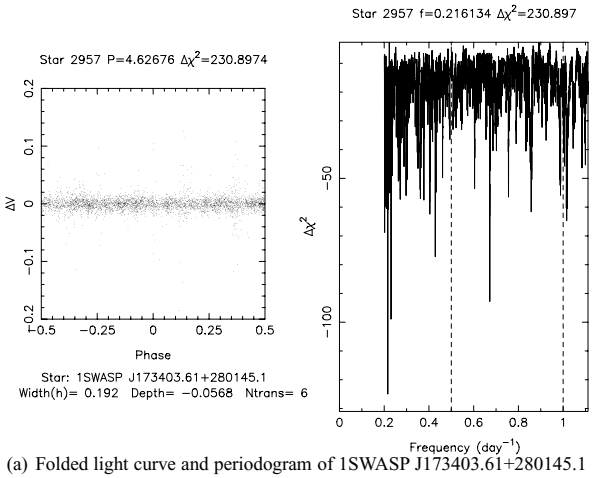

(a) Folded light curve and periodogram of 1SWASP J173403.61+280145.1

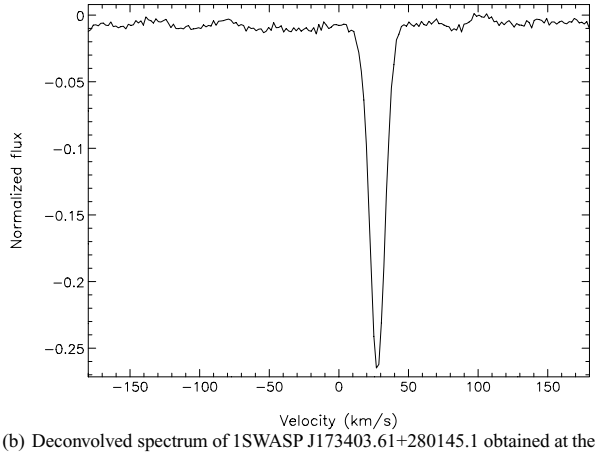

(b) Deconvolved spectrum of 1SWASP J173403.61+280145.1 obtained at the CFHT.

Figure 5. Light curve, periodogram and deconvolved spectrum of 1SWASP J173403.61+280145.1.

5.4.3 1SWASP J173403.61+280145.1

This object was found in the preliminary transit searches but was not identified as a potential candidate in the full data set as there was no convincing evidence of a transit (see Fig. 5a). The reported best period this time ($P = 4.62676$ d) is considerably different from the previous period ($P = 3.72987$ d) based on only two transits, indicating the previous period was probably spurious. There is also no evidence of a periodic signal at the previously detected period with $\Delta\chi^2 > 80$ in any of the top five peaks. In addition, the fitted transit duration is unphysically short (0.192 h) and no evidence of a transit dip is seen in the folded light curves at any of the five alternatives period reported by HUNSTMAN. The deconvolved profiles are shown in Fig. 5(b) and shows a narrow-lined spectrum but with only a single epoch of observation, radial velocity variation cannot be ruled out. It is probably a non-transiting single star.

6 DISCUSSION

6.1 Expected number of transit candidates

From our sample of ∼920 000 stars, approximately 40 per cent have $V \leqslant 13$ enabling SuperWASP to detect a transit, leaving us with ∼370 000 stars. Of these, only a fraction (∼46 per cent – Smith et al. 2006) will have late enough spectral types (F–K) and therefore small enough stellar radii to allow transits to be detected. It is well known that the planet fraction increases with increasing metallicity for solar neighbourhood stars (e.g. Fischer & Valenti 2005) but the metallicities are unknown for our field stars. Assuming a planet fraction of one and a 10 per cent chance of seeing transits from geometric arguments (Horne 2003), we obtain 170 transit candidates assuming 100 per cent observational coverage. The mean number of nights of observation from Table 2 is ∼114, and from examining Fig. 1(b) we can see that we recover >80 per cent of transit candidates with $P < 5$ d if we require four transits to be detected. This drops sharply to ∼20 per cent for $4 > P > 5$ d if we require six transits which is likely to be a minimum number to guarantee a good detection given the presence of correlated noise in the light curves (Pont 2006; Smith et al. 2006). The combination of this factor with others related to the finite observing window and weather effects will reduce the estimate of 170 transit candidates down to ∼20–30, in reasonable agreement with the initial number (58) found given the large uncertainties inherent in the above analysis.

Comparing the transit recovery fraction from a field with 130 nights of observations (e.g. Field SW1743+3126; see Table 2 and

Fig. 1d) and ∼90 nights (e.g. Field SW1745+1028; see Table 2 and Fig. 1a) shows that the fraction recovered drops from ∼80 per cent (for $4 > P > 5$ d) to < 10 per cent. This indicates that it will be necessary to re-observe the same fields covered in the 2004 season in order to increase the observing baseline and the number of detected transits and reduce the correlated systematic noise. The impact of this correlated noise is that fields need to be observed for much longer and substantially more transits are needed for a secure detection than has previously been estimated from simulations which assumed white noise. This will lead to a much lower planet candidate yield for a transit detection experiment than has been thought previously.

6.2 Blending

An additional question is what fraction of our 10 extrasolar planet candidates will turn out to be genuine extrasolar planet candidates after additional follow-up. Many authors have discussed the effects of blending and contamination by eclipsing binaries in both 'wide and shallow' and 'narrow and deep' transit searches and recently Brown (2003) have estimated the contamination rate to be as high as nine out of 10 candidates.

Through our use of filtering on the signal-to-red noise ratio, the transit to antitransit fit ratio and the amount of ellipsoidal variation, combined with the higher resolution 2MASS atlas images to assess blending, we hope to have eliminated the majority of blends caused by grazing incidence and low-mass stellar binaries. The remaining category of blends identified by Brown (2003), namely eclipsing binaries diluted by the light of a foreground or background star, is more difficult to eliminate as has been shown by several authors for different transit search projects (Torres et al. 2004; Mandushev et al. 2005; O'Donovan et al. 2006).

Our strategy of obtaining one or two high-resolution spectroscopic snapshots to rule out blends, begun in a limited fashion as described in Section 2.2, will be able to eliminate this category of false positives more efficiently than through the use of multicolour photometry. Several of the potential candidates could be eliminated with a single ∼10 min exposure when the broadened or double-lined nature was discovered. This compares very favourably with many hours of high-precision multicolour photometry needed to eliminate transit candidates on the basis of unequal eclipse depths in different passbands.

7 CONCLUSIONS

We have conducted a transit search on 13 fields in the RA range 17–18 h and extracted ∼186 000 stars for transit searching. From these stars, we find 9847 initial transit candidates, with 199 of these passing visual inspection. Following filtering, this number was reduced to 58 and with analysis of the blending and the region around each star and the estimated planetary radii this number is reduced to 11 extrasolar planet candidates, with two candidates being detected twice in separate fields.

Initial spectroscopic follow-up on two candidates (1SWASP J174645.84+333411.9 and 1SWASP J172826.46+471208.4) which failed the newer, more stringent filtering in Section 4.4 confirmed the effectiveness of this filtering as these candidates were clearly identified as stellar binaries from the spectra.

These results have been obtained for ∼1/6th of the total number of stars observed by the five cameras of SuperWASP-North over a period of five months. For the 2006 observing season, we will be operating with a total of 16 cameras split over two observing sites. In addition, we expect to be operating the instruments for a greater fraction of the year than in the initial 2004 season, leading to a much greater potential planet catch.

With the large increase in transiting planets expected from operating three times as many cameras, we can look forward to a situation where meaningful statistical comparisons and discrimination between potential planetary models and theories can be made.

NOTE ADDED IN PROOF

Since this paper was accepted, one of the candidates presented here (1SWASP J175207.01+373246.3) has been confirmed to be a planet by the TrES network (O'Donovan et al. 2007).

ACKNOWLEDGMENTS

The WASP consortium consists of representatives from the Queen's University Belfast, University of Cambridge (Wide Field Astronomy Unit), Instituto de Astrofisica de Canarias, Isaac Newton Group of Telescopes (La Palma), University of Keele, University of Leicester, Open University and the University of St Andrews. The SuperWASP-North instrument was constructed and operated with funds made available from the Consortium Universities and the Particle Physics and Astronomy Research Council. SuperWASP-North is located in the Spanish Roque de Los Muchachos Observatory on La Palma, Canary Islands which is operated by the Instituto de Astrofísica de Canarias (IAC). The data reduction and analysis described in this made extensive use of the Starlink Software Collection, without which this project would not have been possible. This research also made use of the SIMBAD data base and VIZIER catalogue service, operated at CDS, Strasbourg, France. In addition, we made use of data products from the 2MASS, which is a joint project of the University of Massachusetts and the Infrared Processing and Analysis Center/California Institute of Technology, funded by the National Aeronautics and Space Administration and the National Science Foundation.

REFERENCES

Agol E., Steffen J., Sari R., Clarkson W., 2005, MNRAS, 359, 567
Alonso R. et al., 2004, ApJ, 613, L153
Ammons S. M., Robinson S. E., Strader J., Laughlin G., Fischer D., Wolf A., 2006, ApJ, 638, 1004
Bakos G., Noyes R. W., Kovács G., Stanek K. Z., Sasselov D. D., Domsa I., 2004, PASP, 116, 266
Bertin E., Arnouts S., 1996, A&AS, 117, 393
Brown T. M., 2003, ApJ, 593, L125
Brown T. M., Charbonneau D., Gilliland R. L., Noyes R. W., Burrows A., 2001, ApJ, 552, 699
Burke C. J., Gaudi B. S., DePoy D. L., Pogge R. W., 2006, AJ, 130, 210
Burrows A., Sudarsky D., Hubbard W. B., 2003, ApJ, 594, 545
Charbonneau D., Brown T. M., Latham D. W., Mayor M., 2000, ApJ, 529, L45
Charbonneau D., Brown T. M., Noyes R. W., Gilliland R. L., 2002, ApJ, 568, 377
Charbonneau D. et al., 2005, ApJ, 626, 523
Christian D. J. et al., 2006, MNRAS, 372, 1117
Collier Cameron A., Horne K., Penny A., Leigh C., 2002, MNRAS, 330, 187
Collier Cameron A. et al., 2006, MNRAS, 373, 799
Cox A. N., 2000, Allen's Astrophysical Quantities, 4th edn. Springer-Verlag, New York

Currie M. J., Berry D. S., 1999, Starlink User Note 95.14, KAPPA. Rutherford Appleton Laboratory
Deming D., Seager S., Richardson L. J., Harrington J., 2005, Nat, 434, 740
Deming D., Harrington J., Seager S., Richardson L. J., 2006, ApJ, 644, 560
Donati J.-F., 2003, in Trujillo-Bueno J., Sanchez Almeida J., eds, ASP Conf. Ser. Vol., 307. Solar Polarization ESPaDOnS: An Echelle SpectroPolarimetric Device for the Observation of Stars at CFHT. Astron. Soc. Pac., San Francisco, p. 41
Donati J.-F., Collier Cameron A., 1997, MNRAS, 291, 1
Donati J.-F., Semel M., Carter B., Rees D. E., Collier Cameron A., 1997, MNRAS, 291, 658
Draper P. W., Taylor M., Allan A., 2002, Starlink User Note 139.16, CCDPACK. Rutherford Appleton Laboratory
Fischer D. A., Valenti J., 2005, ApJ, 622, 1102
Gray D. F., 1992, The Observation and Analysis of Stellar Photospheres, 2nd edn. Cambridge Univ. Press, Cambridge
Høg E. et al., 2000, A&A, 357, 367
Horne K., 2003, in Deming D., Seager S., eds, ASP Conf. Ser. Vol., 294. Scientific Frontiers in Research on Extrasolar Planets Status and Prospects of Planetary Transit Searches: Hot Jupiters Galore. Astron. Soc. Pac., San Francisco, p. 361
Kovács G., Zucker S., Mazeh T., 2002, A&A, 391, 369
Laughlin G., Wolf A., Vanmunster T., Bodenheimer P., Fischer D., Marcy G., Butler P., Vogt S., 2005, ApJ, 621, 1072
Mandushev G. et al., 2005, ApJ, 621, 1061
Mayor M., Queloz D., 1995, Nat, 378, 355
Monet D. G. et al., 2003, AJ, 125, 984
O'Donovan F. T. et al., 2006, ApJ, 644, 1237
O'Donovan F. T. et al., 2007, ApJL, in press (arXiv:0705.2004)
Pollacco D. L. et al., 2006, PASP, 118, 1407
Pont F., 2006, in Arnold L., Bouchy F., Moutou C., eds, Tenth Anniversary of 51 Peg-b: Status of and Prospects for Hot Jupiter Studies. Frontier Group, Paris, p. 153
Protopapas P., Raul J., Alcock C., 2005, MNRAS, 362, 460
Shortridge K., Meyerdierks H., Currie M., Clayton M., Lockley J., Charles A., Davenhall C., 1995, Starlink User Note 86.11, FIGARO. Rutherford Appleton Laboratory
Skrutskie M. F. et al., 2006, AJ, 131, 1163
Smith A. M. S. et al., 2006, MNRAS, 373, 1151
Tamuz O., Mazeh T., Zucker S., 2005, MNRAS, 356, 1466
Tingley B., 2003, A&A, 403, 329
Tingley B., Sackett P. D., 2005, ApJ, 627, 1011
Torres G., Konacki M., Sasselov D. D., Jha S., 2004, ApJ, 614, 979
Udalski A. et al., 2002a, Acta Astron., 52, 1
Udalski A., Zebrun K., Szymanski M., Kubiak M., Soszynski I., Szewczyk O., Wyrzykowski L., Pietrzynski G., 2002b, Acta Astron., 52, 115
Udalski A., Szewczyk O., Zebrun K., Pietrzynski G., Szymanski M., Kubiak M., Soszynski I., Wyrzykowski L., 2002c, Acta Astron., 52, 317
Vidal-Madjar A., Lecavelier des Etangs A., Désert J.-M., Ballester G. E., Ferlet R., Hébrard G., Mayor M., 2003, Nat, 422, 143
Vidal-Madjar A. et al., 2004, ApJ, 604, L69
Wolszczan A., Frail D. A., 1992, Nat, 355, 145

This paper has been typeset from a TEX/LATEX file prepared by the author.